Article

Microstructure, Hardness Evolution, and Thermal Stability Mechanism of Mechanical Alloyed Cu-Nb Alloy during Heat Treatment

Ruoshan Lei [1],*, Mingpu Wang [2], Shiqing Xu [1], Huanping Wang [1] and Guangrun Chen [1]

[1] College of Materials Science and Engineering, China Jiliang University, Hangzhou 310018, China; sxucjlu@cjlu.edu.cn (S.X.); wanghuanping@cjlu.edu.cn (H.W.); cgrzdd@163.com (G.C.)
[2] School of Materials Science and Engineering, Central South University, Changsha 410083, China; wangmp@csu.edu.cn
* Correspondence: leiruoshan@cjlu.edu.cn; Tel.: +86-571-8683-5781

Abstract: The microstructure, hardness evolution, and thermal stability of mechanically alloyed (MA-ed) nanocrystalline Cu–10 wt %Nb solid solution during heat treatment were examined using X-ray diffraction (XRD), scanning electron microscopy (SEM), transmission electron microscopy (TEM), high-resolution TEM (HRTEM) observations, and microhardness measurement. It is found that the pronounced precipitation of Nb from the Cu-Nb supersaturated solid solution occurs at temperatures up to 700 °C, and the annealed alloy shows a bi-nanostructure with Nb nanoparticles dispersed in the nanocrystalline Cu matrix. The bi-nanostructure remains stable with Cu crystalline grain size below 100 nm and Nb particle size around 10 nm even after annealing at 900 °C for 3 h. The microhardness of the annealed sample shows a small increase after annealing at 400 °C, and then it shows a slow decreasing trend with further increasing temperatures. With the help of the kinetics analyses, it is found that the coarsening of the stable Nb nanoparticles is controlled by volume diffusion. The enhanced stability of the nanocrystalline Cu microstructure is mainly attributed to the solute drag and precipitate pinning effects.

Keywords: mechanical alloying; nanocrystalline material; copper alloys; microstructure; high thermal stability

1. Introduction

Nanocrystalline materials have drawn considerable attention due to their excellent mechanical and functional properties [1–4]. The ultrafine grain size and the extremely large number of grain boundaries are generally considered to contribute to these improved properties [3,4]. Therefore, a high thermal stability to minimize the grain growth is required for nanocrystalline materials. There are some techniques to synthesize nanocrystalline materials, one of which is mechanical alloying [5–8]. The generation of the nanostructure is related to the repeated cold welding, fracturing, and mechanical deformation of powder particles in ball-powder-ball and ball-powder-container wall collisions [5,7]. Meanwhile, the enhanced diffusion between two or more elements can be achieved to extend the solid solubility level by using MA [6,8]. Over the past few years, many nanocrystalline materials synthesized by MA have been found to possess a certain thermal stability, although it is often thought that the nanocrystalline materials may offer a significant driving force for the grain growth [9–12]. For example, Chookajorn et al. reported that the MA-ed W-20 at. %Ti powders retained an almost unchanged average grain size of about 24 nm after annealing at 1100 °C for one week. They emphasized the stabilization effect of alloying element, and proposed that the nanostructured W-Ti alloy had a lower free energy

than the coarse grain one [9]. Except stabilizing nanostructures by alloying, the impurity and internal strain introduced by the processing of the materials are also reported to associate with the grain growth suppression [5,11]. By and large, many investigations have been performed to understand the underlying mechanisms for the thermal stability enhancement of nanocrystalline materials; however, some open issues remain to be solved up to now. Especially, the relationship between the microstructure and the thermal stability of nanocrystalline materials still lacks understanding.

The nanocrystalline Cu-Nb alloys prepared by MA have been proved to be a promising conductor due to their high mechanical strength and high electrical conductivity [13–17]. It was demonstrated that the MA-ed Cu-Nb powder mixtures developed a fine nanostructure with Cu grain size of 10 nm or so provided the appropriate processing variables were applied [18–22]. Garroni et al. proposed that the large difference in hardness between Cu and Nb benefited the grain size refinement [7]. Meanwhile, it was reported that up to 10 at. %Nb (corresponding to 14 wt %Nb) could be dissolved within the Cu matrix by MA, though the Cu–Nb phase diagram shows a negligibly low mutual solubility in the solid state [18,20]. After heat treatment, the Nb particles were precipitated sufficiently to improve the strength of the alloys without a significant loss of electrical conductivity [13–18]. E. Botcharova et al. showed that MA-ed Cu-5 at. %Nb alloy had a high mechanical strength of about 1 GPa and a relatively good conductivity of about 50%IACS after annealing at 900 °C for 1 h [13]. More interestingly, it was reported that the Cu nanocrystalline grains of Cu-Nb alloys were quite stable against coarsening with size remaining at about 50 nm even after 10 h at 1000 °C ($\approx$0.92 T_{m}, where T_{m} is the melting temperature of Cu), while the Nb precipitates grew fast to about 500 nm [13,23]. The substantially enhanced stability of MA-ed Cu-Nb alloys has also been reported by other more recent studies [16,19]. However, the microstructural evolution of Cu-Nb alloys during heat treatment still lacks directly experimental observations. Moreover, no mechanisms for the anomalously high thermal stability of the nanocrystalline microstructure in Cu-Nb alloys have been offered yet.

In the present paper, the evolutions of microstructure and microhardness of the MA-ed Cu-Nb powders during heat treatment have been investigated by means of XRD, SEM, TEM, HRTEM observations and microhardness testing. The relationship between the microstructure and microhardness has been analyzed. The growth mechanism of Nb particles is studied from the kinetic viewpoint. The contributions of Nb solute atoms and Nb precipitates in stabilizing the nanostructure of Cu-Nb alloy are assessed.

2. Materials and Methods

2.1. Materials Preparation

The raw materials used were Cu powder (>99.6 wt % pure) of about 50 μm size and Nb powder (>99.4 wt % pure) of about 10 μm size. The Cu-Nb alloy with Nb content of 10 wt % (corresponding to about 10.4% by volume and about 6.9 at. %) was prepared by MA in a QM-1SP4 planetary ball mill (Nanjing University Instrument Plant, Nanjing, China) with stainless steel containers and balls using a rotational speed of 300 rpm at a constant rotation direction and a powder-to-ball weight ratio of 1:14. The milling operation was carried out under argon atmosphere at room temperature until a nanocrystalline supersaturated Cu-Nb solid solution with 10 wt % Nb was formed, i.e., 100 h (detail contents can be seen in [21]). After 100 h milling, the specimens were annealed at constant temperatures from 300 °C up to 900 °C each under an argon atmosphere and for times ranging from 1 h to 3 h.

2.2. Materials Characterization

The XRD measurements were performed on a DMAX2000 X-ray diffractometer (Rigaku Corporation, Tokyo, Japan) with CuK$_{\alpha}$ radiation. To understand the phase evolutions during heat treatment, XRD patterns were obtained in a relatively narrow range of 2θ between 38° and 54° in a relatively slow step size of 0.002° and a scan rate of 0.01°/s. The average grain size and internal

strain of the Cu matrix were determined by Williamson-Hall method after fitting the XRD profile by the Pearson-VII function (detailed information can be found in [21]). SEM study was performed by a Sirion 200 scanning electron microscope (The Netherlands FEI Company, Hillsboro, OR, USA). SEM samples were embedded in conductive resin and prepared by standard metallographic techniques. TEM investigation was carried out using a FEI TecnaiG2 (The Netherlands FEI Company, Hillsboro, OR, USA) operating at 200 KV. In some cases, when a higher resolution was needed, HRTEM was performed on a JEOL JEM-2100 (JEOL Company, Tokyo, Japan) operating at 200 kV with a point resolution of 1.9 Å. TEM samples were prepared by the method which involves mechanical grinding, conventional dimpling, and ion beam milling. A Gatan Digital Micrograph software (Version 3.11.2, Gatan Company, Pleasanton, CA, USA) was applied to measure the sizes of Cu grains and Nb particles from the TEM and SEM images. At least 150 Cu grains and 100 Nb particles were measured for each sample, from which the size distributions were calculated. Microhardness tests were carried out using a load of 2 Kg and holding for 30 s on a HVA-10A Vickers microhardness tester (Laizhou Instrument Plant, Laizhou, China).

3. Results

3.1. XRD Analysis

Figure 1a shows the XRD patterns of MA-ed Cu-10 wt %Nb solid solution after annealing at different temperatures for 1 h. For comparison, the corresponding pattern of as-milled powder is also given. It can be seen that Cu diffraction peaks have undergone a height increase and a breadth decrease with the increase of annealing temperatures, which can be attributed to the growth of Cu grains and the reduction of internal strain. Meanwhile, a shift of Cu peaks towards higher angles can be observed, indicating the contraction of the Cu lattice during heat treatment. After annealing at 600 °C, a small peak from Fe_7Nb_6 phase is detected. The impurity of Fe results from the abrasions of the milling vessels and balls during milling. Similar results have also been reported by E. Botcharova et al. for Cu-Nb powders milled at liquid nitrogen temperature [20]. A temperature of 700 °C leads to the appearance of $(110)_{Nb}$ peak, which becomes more pronounced with increasing temperature. In addition, high annealing temperatures result in the formation of CuO phase. The contamination of oxygen is hard to avoid completely during milling, although the milling process was performed under an argon atmosphere.

Figure 1b shows the crystalline grain size and internal strain of the Cu matrix determined from the XRD data. It reveals that the Cu crystalline grain size of the as-milled sample is only 9 nm. The Cu grain size of 400 °C annealed sample increases little, indicating the good stabilizing effect from Nb. At higher annealing temperatures, the increase of Cu grain size gradually speeds up, especially above 600 °C. The Cu grain size increases to 24 nm at 600 °C and 55 nm at 900 °C. Meanwhile, the corresponding internal strain of Cu matrix decreases with increasing annealing temperature, suggesting the occurrence of the recovery process. The internal strain reduces to only 0.23% after annealing at 900 °C for 1 h.

In order to investigate the precipitation of Nb atoms from the Cu matrix, the evolution of Cu lattice parameter as a function of temperatures is presented in Figure 1c. It can be seen that the lattice parameter of the Cu matrix decreases with the annealing temperatures. After being annealed at 900 °C for 1 h, the Cu lattice parameter decreases to reach the value of pure copper (0.3615 nm [10]). Such change in Cu lattice parameter is only possible when Nb precipitates from the Cu matrix due to the larger atomic size of Nb than Cu.
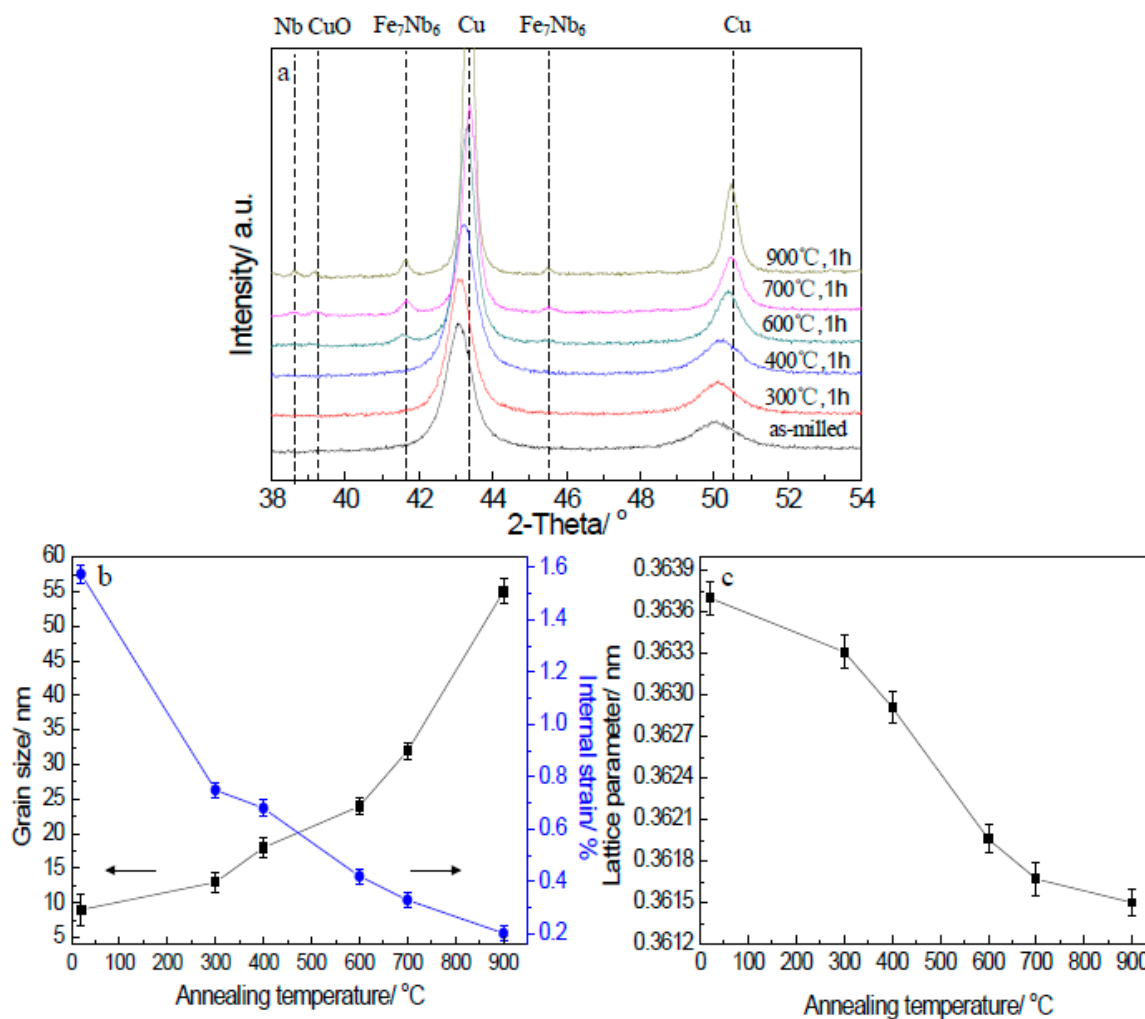
Figure 1. XRD results of MA-ed Cu-Nb powders after annealing at different temperatures for 1 h. (**a**) XRD patterns of annealed samples; (**b**) Mean crystalline grain size (indicated by left arrow) and internal strain of Cu phase (indicated by right arrow) with respect to annealing temperatures; (**c**) Cu lattice parameter as a function of annealing temperatures.

3.2. SEM Observations

Figure 2 shows the SEM images of MA-ed Cu-Nb powders after annealing under different conditions. It can be seen that there is no significant change in the solid solution and little Nb precipitates can be detected in the view after annealing at 400 °C for 1 h (Figure 2a). Obvious precipitation from the solid solution starts at 700 °C (Figure 2b). Since the atomic number of Cu ($Z = 29$) is smaller than that of Nb ($Z = 41$), the light regions are Nb-rich particles while the grey regions are the Cu matrix. With further increasing temperature, the number and the size of Nb precipitates increase. Coarsening of the precipitates leads to a size of 100–250 nm at 900 °C for 1 h (Figure 2c) and 150–350 nm at 900 °C for 3 h (Figure 2d), respectively.
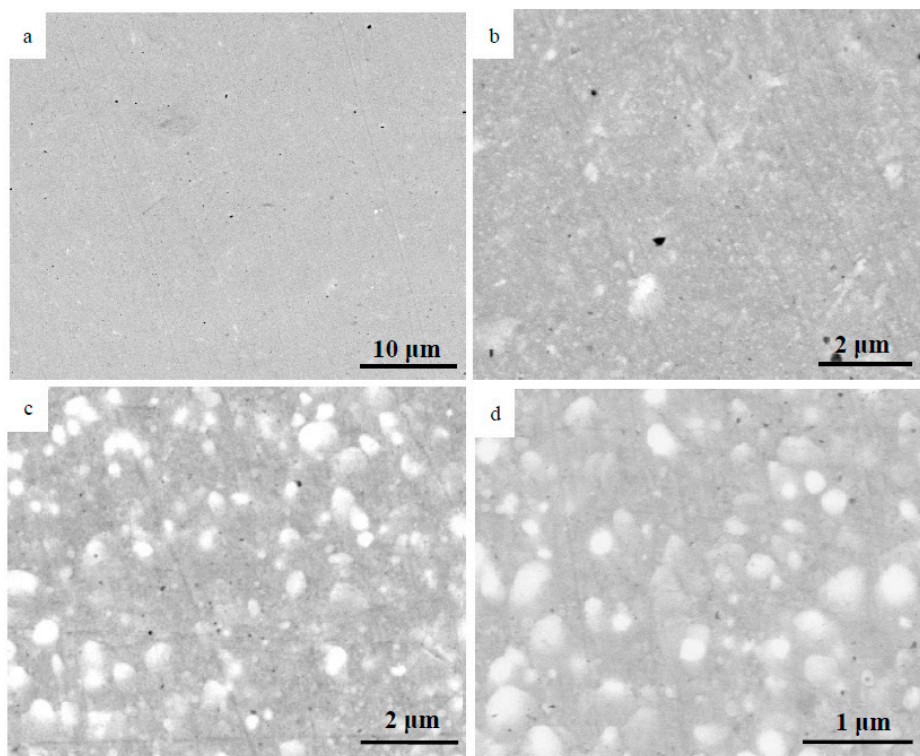
Figure 2. SEM images of MA-ed Cu-Nb powders annealed under different conditions: (**a**) 400 °C, 1 h; (**b**) 700 °C, 1 h; (**c**) 900 °C, 1 h; (**d**) 900 °C, 3 h.

3.3. TEM Observations

Figure 3 shows the microstructure of MA-ed Cu-Nb powders after annealing at 400 °C for 1 h observed by TEM. It can be seen that the nanocrystalline grain microstructure and the strain-contrast induced by milling are maintained (Figure 3a). The histogram with the statistical Cu grain size distribution reveals that the average size is about 14 nm (Figure 3b), which is in a good agreement with the value obtained by the XRD analysis. The electron diffraction patterns (EDP) have been carried out, and few faint rings with bright spots contributed from Nb phase appear (Figure 3c), which confirms that some Nb atoms have precipitated from the solid solution. However, no obvious Nb clusters or nanosized Nb precipitates have been detected by TEM due to their small sizes and the strain contrast. In order to obtain further information, the HRTEM observations were conducted. Figure 3d shows a HRTEM image of a Nb-rich cluster with size of around 3 nm, which displays a darker contrast than the surrounding Cu matrix. The corresponding Fourier-filtered image of Figure 3d shows that the Nb-rich cluster appears to be fully coherent with the surrounding Cu matrix and has the same two-dimensional lattice (Figure 3e), which suggests that the Nb-rich cluster may have the same FCC lattice as that of the Cu matrix.

After annealing at 700 °C for 1 h, the average Cu crystalline grain size increases to about 34 nm (Figure 4a,b). Meanwhile, Nb precipitates with the average size of about 4 nm are distributed in the Cu matrix. Some of the Nb nanosized precipitates are located in the grain boundaries, while others are dispersed inside the Cu nano-grains (Figure 4c). Therefore, the microstructure of MA-ed Cu-Nb alloys after heat treatment consists of Nb nano-precipitates dispersed within the nanocrystalline Cu matrix, namely a unique bi-nanostructure is formed. Moreover to this, in dark field (DF) mode (Figure 4d), it is obvious that some regions of the grain boundary are extremely bright (as marked by the white arrow), indicating the segregation and accumulation of Nb atoms along the grain boundary after heat treatment. The evidence of Nb solute segregation reminds us that the effect of Nb solute segregation

on the thermal stability enhancement of MA-ed Cu-Nb alloys should be analyzed in detail, which has been ignored in the past investigations.
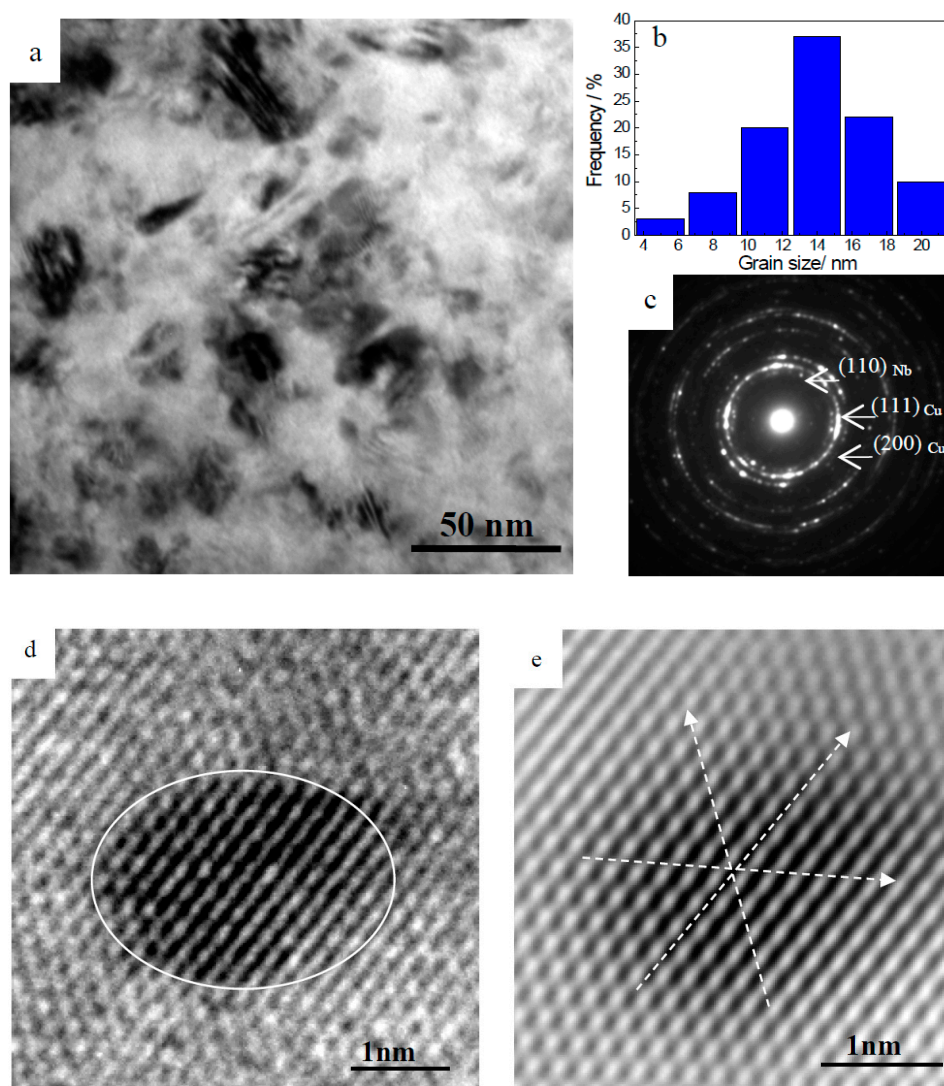

Figure 3. TEM and HRTEM images of MA-ed Cu-Nb powders annealed at 400 °C for 1 h. (**a**) bright field (BF) image; (**b**) Cu grain size distribution histogram; (**c**) EDP; (**d**) HRTEM image of a Nb-rich cluster, which is outlined by the white line; (**e**) the corresponding Fourier-filtered image of Figure (**d**). White arrows were superimposed on different lattice planes to indicate their position.

The TEM images of MA-ed Cu-Nb powders after annealing at 900 °C for different times are presented in Figure 5. From Figure 5a,b, it can be seen that the Cu-Nb powders retain a uniform nanostructure with an average size of about 57 nm after annealed at 900 °C for 1 h. When the annealing time prolongs to 3 h, Cu grains still grow slowly, and the Cu grain size is smaller than 100 nm (Figure 5c,d). Meanwhile, the dispersed Nb nanoparticles have a high stability with sizes of 5–20 nm (Figure 5e). Furthermore, Botcharova et al. proved that the Cu-10 at. % Nb alloy kept a fine nanocrystalline structure even after annealing at 1000 °C for 10 h. Hence, it can be suggested that the MA-ed nanocrystalline Cu-Nb system is quite stable over long durations at elevated temperatures.
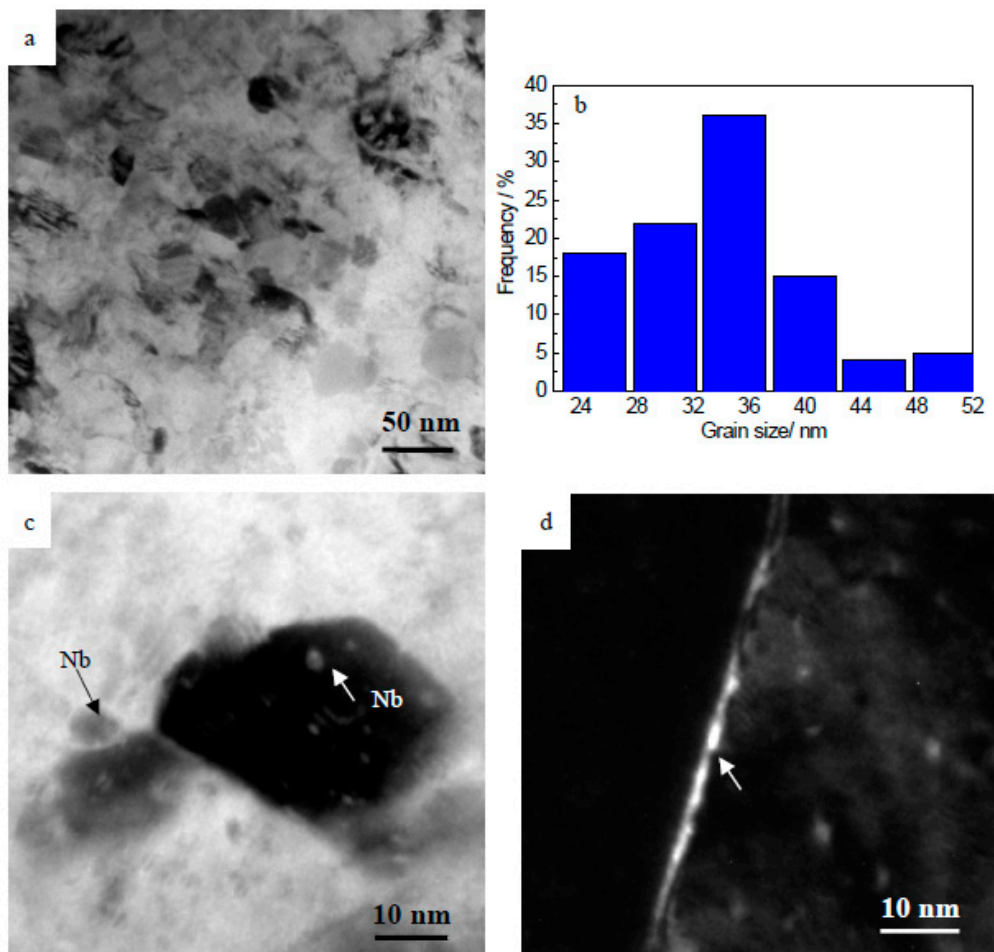
Figure 4. TEM images of MA-ed Cu-Nb powders annealed at 700 °C for 1 h. (**a**) BF image, nanocrystalline Cu grains; (**b**) Cu grain size distribution histogram; (**c**) BF image, Nb nanoparticles; (**d**) DF image, which is formed by selecting one part of the $(110)_{Nb}$ reflection. The segregation at grain boundary is indicated by the arrow.
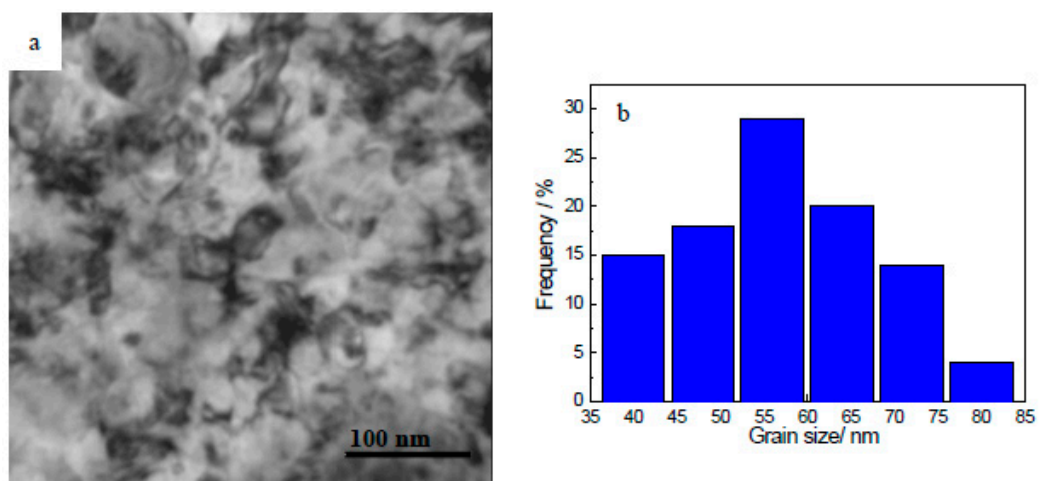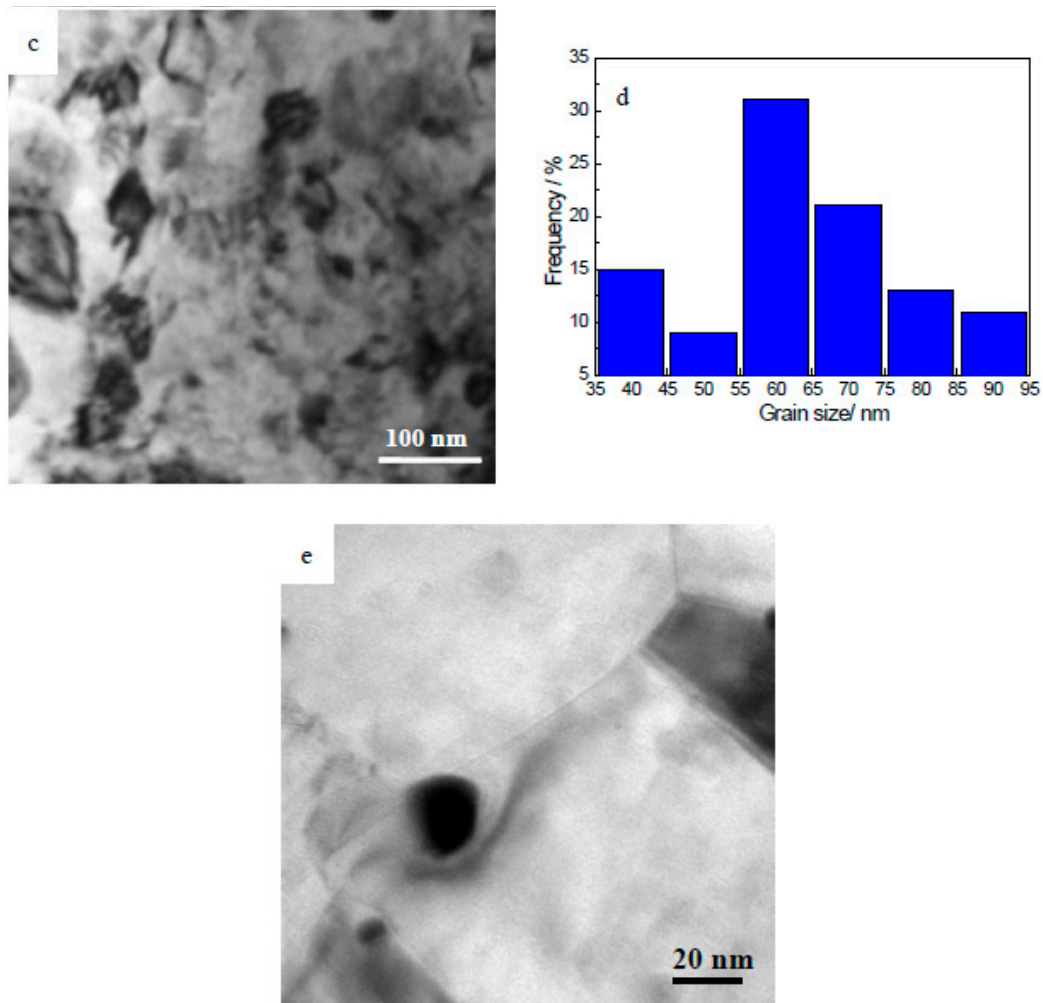

Figure 5. *Cont.*

Figure 5. TEM images of MA-ed Cu-Nb powders annealed at 900 °C. (**a**) 1 h, BF image, nanocrystalline Cu grains; (**b**) 1 h, Cu grain size distribution histogram; (**c**) 3 h, BF image, nanocrystalline Cu grains; (**d**) 3 h, Cu grain size distribution histogram; (**e**) 3 h, BF image, Nb nanoparticles.

3.4. Microhardness Measurements

Figure 6 shows the effect of annealing temperatures on the microhardness of MA-ed Cu-Nb powders. For statistical reasons, 10 indents were made over the whole specimen area to obtain an average value. For the as-milled sample, the microhardness is about 460 HV. There is a slight decrease in the microhardness of the powders when the annealing was carried out beyond 300 °C. With increasing annealing temperature, the microhardness increases and reaches a peak hardness of 441 HV at 400 °C. Although the recovery process leads to the decrease of microhardness, the formation of Nb clusters can contribute to an increase of the microhardness. At temperature of 400 °C, the strengthening effect caused by the formation of Nb clusters is higher than the softening effect of the recovery process. Therefore, the microhardness value reaches a maximum value. A further increase of the annealing temperature results in a slow decrease of the microhardness, which may be attributed to the Cu grain growth and the precipitation coarsening. After annealing at 900 °C for 1 h, the microhardness decreases to about 375 HV, which is still quite high compared to that of pure Cu. The above changes indicate that the alloy has a high resistance to softening at elevated temperatures.
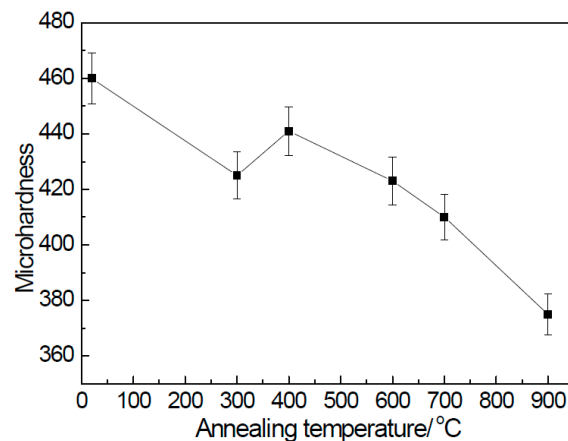
Figure 6. The microhardness of MA-ed Cu-Nb powders after annealing at different temperatures for 1 h.

On the other hand, the microhardness of the metallic materials is closely related with their microstructures. Based on the microstructural characterization presented above (Figures 1–5), solid solution strengthening for the sample annealed at the temperatures above 600 °C becomes less important owing to the precipitation of Nb from the Cu matrix. In addition, dislocation strengthening is not significant as the internal strain is reduced to minor levels at high temperatures. As the microstructure of the annealed Cu-10 wt %Nb powders is built from Nb nanoparticles dispersed within the nanocrystalline Cu matrix, we suggest that the strengthening mechanisms are mainly based on the nanocrystalline grains according to the Hall-Petch relation and the nanoparticles referring to the precipitation strengthening [17].

4. Discussion

As illustrated above, the microstructure of MA-ed Cu-Nb powders is quite stable at elevated temperatures. Even after annealing at 900 °C for 3 h, the size of the Nb nanoparticles is still 5–20 nm, and the structure of the Cu matrix remains nanocrystalline with grain size below 100 nm. The slow growth of the nanocrystalline Cu grains is in agreement with the results reported by other investigators [13,16,18,19]. Nevertheless, E. Botcharova et al. demonstrated that a fast coarsening of the Nb particles led to a size of 150–350 nm at 900 °C for 1 h, and suggested that the sub-micron sized Nb particles could not hinder the Cu grain growth due to their much larger size than that of Cu grains [13,18,23]. By far, the high thermal stability of the nanocrystalline structure in Cu-Nb alloys has not yet been explained reasonably. In this section, our basic interest is to discuss the thermal stability mechanisms for the MA-ed Cu-Nb alloy.

4.1. Stability of Nb Nanoparticles

Based on the SEM and TEM observations (Figures 2–5), the sizes of Nb particles show a bimodal distribution. Considering the resolution limits of TEM and SEM techniques, the sizes of Nb particles smaller than 50 nm were measured from TEM images, and the corresponding size histograms for the Cu-Nb powders annealed at different temperatures are shown in Figure 7. Instead, the SEM examinations have given the information about the particles with sizes larger than 50 nm (Figure 8). From these experimental size histograms, the average Nb particle sizes ($\Phi_{Nb,SEM}$ and $\Phi_{Nb,TEM}$) after annealing under different conditions are illustrated in Table 1. Apparently, the fine Nb nanoparticles can help reduce the growth of the nanocrystalline Cu matrix through precipitate pinning effect, while the large Nb particles with size above 50 nm may have no contribution to the enhanced thermal stability. Therefore, it is necessary to consider the coarsening mechanisms of the Nb particles.
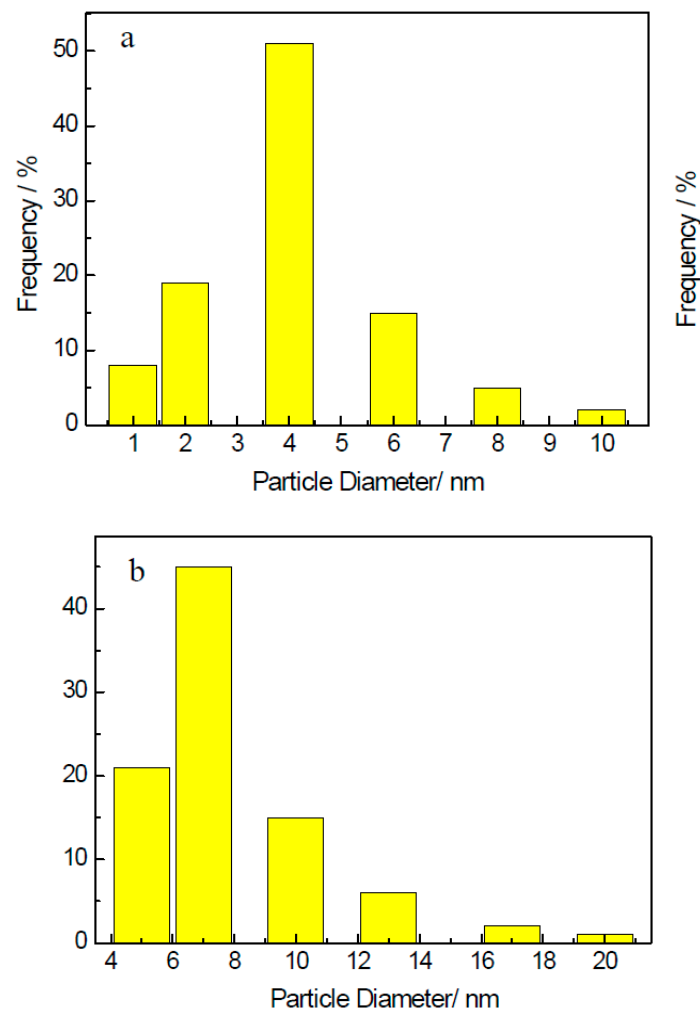
Figure 7. Histograms of Nb particle sizes detected from TEM images showing the Nb particles with sizes less than 50 nm. (**a**) annealed at 700 °C for 1 h; (**b**) annealed at 900 °C for 1 h.

Table 1. Summary of Nb particle sizes after annealing under different conditions. (Note: $\Phi_{\text{Nb,SEM}}$ is the average Nb particle size observed by SEM, and $\Phi_{\text{Nb,TEM}}$ is the average Nb particle size measured by TEM).

Preparation	400 °C, 1 h	700 °C, 1 h	900 °C, 1 h	900 °C, 3 h
$\Phi_{\text{Nb,SEM}}$ (nm)	No	78	175	207
$\Phi_{\text{Nb,TEM}}$ (nm)	No	4	7	11

In general, the kinetics of the particle coarsening by volume diffusion can be described by the Lifshitz-Slyozov-Wagner (LSW) equation [24–26]. It is expressed as follows:

$$r^3 - r_0^3 = \left(\frac{8}{9}\right)\left(\frac{\gamma C V D t}{RT}\right) \tag{1}$$

where r_0 and r are the initial and final particle radii, respectively, γ is the interface energy of the Cu-Nb interface ($\gamma_{\text{Cu-Nb}} = 0.1\,\text{J·m}^{-2}$ [15]), C is the solubility of Nb solute in Cu at temperature T, V is the molar volume of the Nb phase ($V_{\text{Nb}} = 10.8 \times 10^{-6}\,\text{m}^3\text{·moL}^{-1}$), D is the diffusivity of solute in the solvent, R is the gas constant, and t the annealing time. Taking the particles coarsening from initial solution with an initial particle size of zero, describing the solubility of Nb in Cu using a regular solution model with a solubility of 0.1% at 1080 °C [27], given the diffusivity of Nb in Cu by an Arrhenius-type

expression $D = D_0 \exp(-Q/RT)$ with a pre-exponential term of value 2×10^{-4} m^2·s^{-1} and an activation energy of 249 kJ·moL^{-1} [28]. Accordingly, the particle sizes after annealing at 700 and 900 °C for 1 h can be calculated to be about 3 and 9 nm, respectively, as well as 13 nm after annealing at 900 °C for 3 h. These calculated values are in good agreement with the measured data (as shown in Table 1), confirming that the growth of these extremely fine nanoparticles is controlled by volume diffusion coarsening.
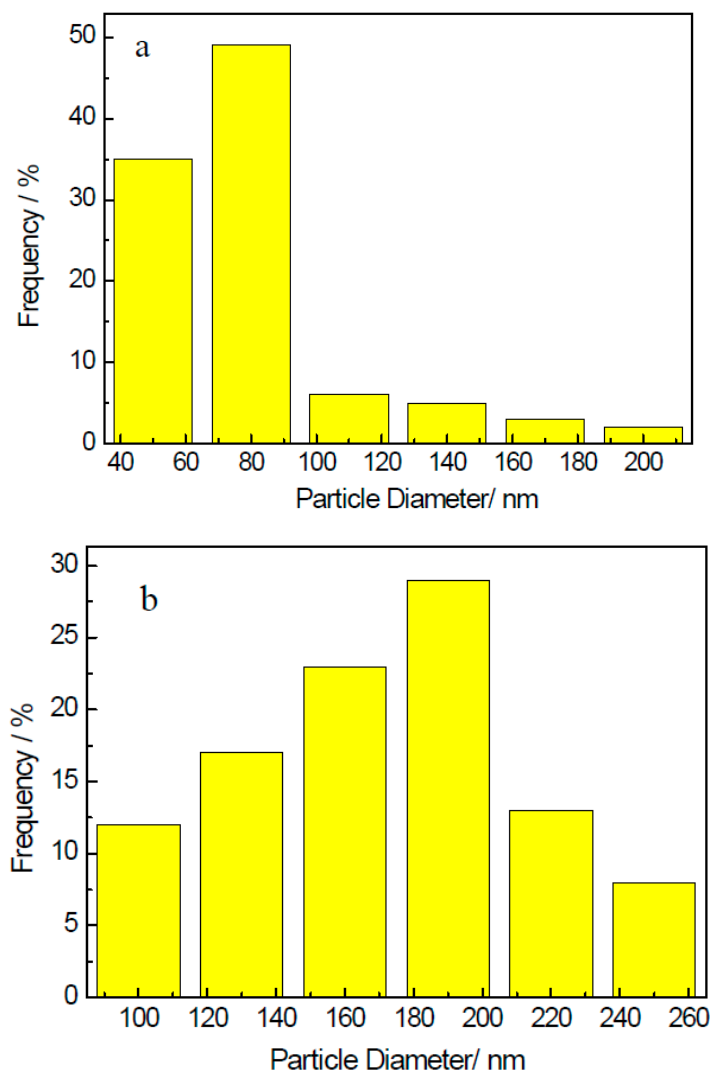

Figure 8. Nb particle size histograms obtained from SEM images showing the Nb particles larger than 50 nm. (**a**) annealed at 700 °C for 1 h; (**b**) annealed at 900 °C for 1 h.

Nevertheless, the LSW coarsening theory cannot explain the rapid growth of the large Nb particles with size above 50 nm as observed by SEM. Since the grain boundary is one of the main defects in the nanocrystalline Cu matrix, the rapid mass transport along the grain boundaries may contribute to the rapid growth of large Nb particles. In this case, the coarsening of the particles varies according to [29]:

$$r^4 - r_0^4 = \left(\frac{8}{9}\right)\left(\frac{\gamma C V D t}{RT}\right) \tag{2}$$

As the grain boundary diffusivity, thickness, and energy are all poorly defined, additional approximations should be made to estimate these parameters. Assuming that the activation energy for grain boundary diffusion is about 0.6 that for bulk diffusion [28,30], that the grain boundary

thickness is about 1–1.5 nm [30], that the grain boundary energy is about equal to that of the Cu-Nb interface energy, we calculated that the particle size after annealing at 700 and 900 °C for 1 h is about 70 and 160 nm, respectively, as well as 210 nm after annealing at 900 °C for 3 h, which are in agreement with the experimental observations. Therefore, the growth of these large Nb particles is suggested to be controlled by grain boundary diffusion coarsening.

4.2. Stability of the Nanocrystalline Cu Matrix

For the MA-ed Cu-Nb alloy investigated, Cu nanocrystalline grains show a significant enhanced resistance against grain growth. The reasons for the high thermal stability should be found. It has been widely reported that "Zener drag" of the particles can hinder the grain growth of the matrix [31]. Besides, the mechanism of solute segregation has also been suggested to impart thermal stability to nanocrystalline materials [32,33]. Therefore, we evaluate the potential contributions of the two mechanisms towards the thermal stability of MA-ed Cu-Nb powders.

Analysis of the XRD data indicates that, for the samples annealed at temperatures below 600 °C, a large number of Nb atoms are still dissolved in the Cu matrix and the Cu grain growth rate is slow (Figure 1). Nevertheless, the Cu grains have experienced a relatively rapid growth when the formation of precipitate phases can be detected at higher temperatures. Such behavior implies that the grain growth rate is limited before obvious phase separation sets in. As Cu-Nb has a negligible mutual solid solubility between each other, excess solute atoms are rejected from the grain interior at elevated temperatures [34]. As a consequence, the segregation of solute atoms to the grain boundaries occurs during the heat treatment of MA-ed supersaturated Cu-Nb solid solution, which is confirmed by TEM observation (Figure 4d). Therefore, it can be suggested that the high concentration of Nb atoms residing in the grain boundaries can suppress the grain growth through the hindrance of the migration of the Cu grain boundaries due to the solute drag effect [35].

On the other hand, TEM observation has shown that a large amount of nanoparticles are dispersed within the annealed Cu-Nb powders. The potential effectiveness of these nanoparticles to suppress the grain growth as grain pinning points can be evaluated using the Hillert-Gladman equation, which relates the average grain size with the volume fraction and size of nanoparticles [36]. The equation is written as:

$$d = 3/2 \cdot D f_{\text{v}} \tag{3}$$

where d is the pinning particle size, D is the grain size, and f_{v} is the volume fraction of the particles. As mentioned above, the large particles with sizes above 50 nm cannot hinder the Cu nanocrystalline grain growth. However, the volume fraction of Nb particles with sizes below 50 nm can be not estimated by TEM due to the uncertainty of the thickness of the thin foil and the overlap of particles in the projected TEM images. Furthermore, the CuO and Fe_7Nb_6 particles can also influence the Cu grain growth; unfortunately, their volume fractions are also difficult to obtain. Thus, we are not able to obtain the exact volume fraction f_{v} of the pinning particles. Taking $f_{\text{v}} = 10\%$ for simplicity, for the sample annealed at 700 °C ($D_{\text{Cu}} = 34$ nm) and 900 °C ($D_{\text{Cu}} = 57$ nm) for 1 h, the calculated values of the particle size d are estimated to be about 5.1 nm and 8.5 nm, respectively. The calculated values are very close to the experimentally measured ones (Table 1). Furthermore, the ultrafine nanoparticles also help in the stabilization of Cu grains by hindering dislocation movements as per the Orowan mechanism. Thus, the present results support that the Nb, Fe_7Nb_6, and CuO nanoparticles can act as the primary source of stabilization after most of the solute atoms precipitate from the Cu matrix at high temperatures.

5. Conclusions

1. TEM observations show that the microstructure of the MA-ed nanocrystalline Cu-10 wt %Nb alloy after heat treatment is characterized by nanosized Nb precipitates dispersed in a nanocrystalline Cu matrix. This bi-nanostructure remains stable with Cu grain size below 100 nm and the average Nb

particle size around 10 nm even after annealing at 900 °C for 3 h. Therefore the Cu-Nb alloy shows an unexpectedly high thermal stability.

2. With annealing temperature increasing, the microhardness of MA-ed Cu-10 wt %Nb powders reaches a peak hardness of 441 HV at 400 °C for 1 h, and decreases slowly to 375 HV after annealing at 900 °C for 1 h. The strengthening mechanisms are related with the bi-nanostructure, including nanocrystalline strengthening and precipitation strengthening.

3. The sizes of Nb particles show a bimodal distribution after heat treatment. Using a kinetics analysis, the growth of Nb nanoparticles with size less than 20 nm or so is found to be controlled by volume diffusion coarsening, while the growth of Nb particles with sizes above 50 nm is controlled by grain boundary diffusion.

4. The enhanced thermal stability of MA-ed nanocrystalline Cu-Nb alloy is mainly attributed to the Nb solute atoms and the nanosized Nb precipitates in the Cu matrix, which is associated with the solute drag and precipitate pinning effects.

Author Contributions: Ruoshan Lei and Mingpu Wang conceived and designed the experiments; Ruoshan Lei and Shiqing Xu performed the experiments; Ruoshan Lei and Huanping Wang analyzed the data; Huanping Wang contributed materials and analysis tools; Ruoshan Lei and Guangrun Chen wrote the paper.

Conflicts of Interest: The authors declare no conflict of interest.

References

1. Li, Z.M.; Fu, L.M.; Fu, B.; Shan, A.D. Effects of annealing on microstructure and mechanical properties of nano-grained titanium produced by combination of asymmetric and symmetric rolling. *Mater. Sci. Eng. A* **2012**, *558*, 309–318. [CrossRef]

2. Herzer, G. Modern soft magnets: Amorphous and nanocrystalline materials. *Acta Mater.* **2013**, *61*, 718–734. [CrossRef]

3. Azabou, M.; Khitouni, M.; Kolsi, A. Characterization of nanocrystalline Al-based alloy produced by mechanical milling followed by cold-pressing consolidation. *Mater. Charact.* **2009**, *60*, 499–505. [CrossRef]

4. Lari Baghal, S.M.; Amadeh, A.; Sohi, M.H. Investigation of mechanical properties and operative deformation mechanism in nano-crystalline Ni-Co/SiC electrodeposits. *Mater. Sci. Eng. A* **2012**, *542*, 104–112. [CrossRef]

5. Suryanarayana, C. Mechanical alloying and milling. *Prog. Mater. Sci.* **2001**, *46*, 1–184. [CrossRef]

6. Garroni, S.; Enzoa, S.; Delogu, F. Mesostructural refinement in the early stages of mechanical alloying. *Scr. Mater.* **2014**, *83*, 49–52. [CrossRef]

7. Garroni, S.; Soru, S.; Enzo, S.; Delogu, F. Reduction of grain size in metals and metal mixtures processed by ball milling. *Scr. Mater.* **2014**, *88*, 9–12. [CrossRef]

8. Baláž, P.; Achimovičová, M.; Baláž, M.; Billik, P.; Cherkezova-Zheleva, Z.; Criado, J.M.; Delogu, F.; Dutková, E.; Gaffet, E.; Gotor, F.J.; et al. Hallmarks of mechanochemistry: From nanoparticles to technology. *Chem. Soc. Rev.* **2013**, *42*, 7571–7637. [CrossRef] [PubMed]

9. Chookajorn, T.J.; Murdoch, H.A.; Schuh, C.A. Design of Stable Nanocrystalline Alloys. *Science* **2012**, *337*, 951–954. [CrossRef] [PubMed]

10. Atwater, M.A.; Roy, D.; Darling, K.A.; Butler, B.G.; Scattergood, R.O.; Koch, C.C. The thermal stability of nanocrystalline copper cryogenically milled with tungsten. *Mater. Sci. Eng. A* **2012**, *558*, 226–233. [CrossRef]

11. Akbarpour, M.R.; Kim, H.S. Microstructure, grain growth, and hardness during annealing of nanocrystalline Cu powders synthesized via high energy mechanical milling. *Mater. Des.* **2015**, *83*, 644–650. [CrossRef]

12. Liu, W.B.; Zhang, C.; Xia, Z.X.; Yang, Z.G.; Wang, P.H.; Chen, J.M. Strain-induced refinement and thermal stability of a nanocrystalline steel produced by surface mechanical attritiontreatment. *Mater. Sci. Eng. A* **2013**, *568*, 176–183. [CrossRef]

13. Botcharova, E.; Freudenberger, J.; Schultz, L. Mechanical and electrical properties of mechanically alloyed nanocrystalline Cu–Nb alloys. *Acta Mater.* **2006**, *54*, 3333–3341. [CrossRef]

14. Freudenberger, J.; Botcharova, E.; Schultz, L. Formation of the microstructure in Cu-Nb alloys. *J. Mater. Sci.* **2004**, *39*, 5343–5345. [CrossRef]

15. Benghalem, A.; Morris, D.G. Microstructure and mechanical properties of concentrated copper-niobium alloys prepared by mechanical alloying. *Mater. Sci. Eng. A* **1993**, *161*, 255–266. [CrossRef]

16. Abad, M.D.; Parker, S.; Kiener, D.; Primorac, M.M.; Hosemann, P. Microstructure and mechanical properties of Cu$_x$Nb$_{1-x}$ alloys prepared by ball milling and high pressure torsion compacting. *J. Alloys Comp.* **2015**, *630*, 117–125. [CrossRef]

17. Lei, R.S.; Xu, S.Q.; Wang, M.P.; Wang, H.P. Microstructure and properties of nanocrystalline copper–niobium alloy with high strength and high conductivity. *Mater. Sci. Eng. A* **2013**, *586*, 367–373. [CrossRef]

18. Botcharova, E.; Freudenberger, J.; Schultz, L. Cu–Nb alloys prepared by mechanical alloying and subsequent heat treatment. *J. Alloys Comp.* **2004**, *365*, 157–163. [CrossRef]

19. Mula, S.; Bahmanpour, H.; Mal, S.; Kang, P.C.; Atwater, M.; Jian, W.; Scattergood, R.O.; Kochet, C.C. Thermodynamic feasibility of solid solubility extension of Nb in Cu and their thermal stability. *Mater. Sci. Eng. A* **2012**, *539*, 330–336. [CrossRef]

20. Botcharova, E.; Heilmaier, M.; Freudenbergera, J.; Drew, G.; Kudashow, D.; Martin, U.; Schultz, L. Supersaturated solid solution of niobium in copper by mechanical alloying. *J. Alloys Comp.* **2003**, *351*, 119–125. [CrossRef]

21. Lei, R.S.; Wang, M.P.; Li, Z.; Wei, H.G.; Yang, W.C.; Jia, Y.L.; Gong, S. Structure evolution and solid solubility extension of copper–niobium powders during mechanical alloying. *Mater. Sci. Eng. A* **2011**, *528*, 4475–4481. [CrossRef]

22. Lei, R.S.; Wang, M.P.; Wang, H.P.; Xu, S.Q. New insights on the formation of supersaturated Cu-Nb solid solution prepared by mechanical alloying. *Mater. Charact.* **2016**, *118*, 324–331. [CrossRef]

23. Botcharova, E.; Freudenberger, J.; Schultz, L. High thermal stability of mechanically-alloyed nanocrystalline Cu–Nb alloys. *Int. J. Mater. Res.* **2006**, *97*, 1350–1354. [CrossRef]

24. Lifshitz, I.M.; Slyozov, V.V. The Kinetics of Precipitation from Supersaturated Solid Solutions. *J. Phys. Chem. Solids* **1961**, *19*, 35–50. [CrossRef]

25. Wagner, C. Theorie der Alterung von Niederschlägen durch Umlösen (Ostwald-Reifung). *Z. Elektrochem. Beri. Bunsenges. Physikalische Chem.* **1961**, *65*, 581–591.

26. Barlow, I.C.; Jones, H.; Rainforth, W.M. The effect of heat treatment at 500–655 °C on the microstructure and properties of mechanically alloyed Al-Ti-O based material. *Mater. Sci. Eng. A* **2003**, *351*, 344–357. [CrossRef]

27. Hansen, N.; Anderko, K. *Constitution of Binary Alloys*, 2nd ed.; McGraw-Hill: New York, NY, USA, 1958.

28. Butrymowicz, D.B.; Manning, J.R.; Read, M.E. *Diffusion Rate Data and Mass Transport Phenomena for Copper Systems*, 1st ed.; International Copper Research Association: Washington, DC, USA, 1977.

29. Ardell, A. On the coarsening of grain boundary precipitates. *Acta Metall.* **1972**, *20*, 601–619. [CrossRef]

30. Gjostein, N.A. *Diffusion*, 1st ed.; American Society for Metals: Metals Park, OH, USA, 1973.

31. Humphreys, F.J.; Hatherly, M. *Recrystallisation and Related Annealing phenomena*; Pergamon: Oxford, UK, 1996.

32. Fiedler, H.C. Grain oriented silicon- iron with a unique inhibition system for texture development. *Metall. Trans. A* **1977**, *8*, 1307–1312. [CrossRef]

33. Fan, G.J.; Gao, W.N.; Quan, M.X.; Hu, Z.Q. Preparation and thermal stability of supersaturated nanocrystalline Al-Ti alloys. *Mater. Lett.* **1995**, *23*, 33–37. [CrossRef]

34. Briant, C.L. Solid solubility and grain boundary segregation. *Philos. Mag. Lett.* **1996**, *73*, 345–349. [CrossRef]

35. Frolov, T.; Darling, K.A.; Kecskes, L.J.; Mishin, Y. Stabilization and strengthening of nanocrystalline copper by alloying with tantalum. *Acta Mater.* **2012**, *60*, 2158–2168. [CrossRef]

36. Hillert, M. On the theory of normal and abnormal grain growth. *Acta Metall.* **1965**, *13*, 227–238. [CrossRef]